

Protocaseyite, a new decavanadate mineral containing a $[\text{Al}_4(\text{OH})_6(\text{H}_2\text{O})_{12}]^{6+}$ linear tetramer, a novel isopolycation

ANTHONY R. KAMPF^{1,*}, MARK A. COOPER², JOHN M. HUGHES³, CHI MA^{4,†}, WILLIAM H. CASEY⁵,
FRANK C. HAWTHORNE², AND JOE MARTY¹

¹Mineral Sciences Department, Natural History Museum of Los Angeles County, Los Angeles, California 90007, U.S.A.

²Department of Geological Sciences, University of Manitoba, Winnipeg, Manitoba R3T 2N2, Canada

³Department of Geology, University of Vermont, Burlington, Vermont 05405, U.S.A.

⁴Division of Geological and Planetary Sciences, California Institute of Technology, Pasadena, California 91125, U.S.A.

⁵Department of Chemistry, Department of Earth and Planetary Sciences, University of California at Davis, Davis, California 95616, U.S.A.

ABSTRACT

Protocaseyite, $[\text{Al}_4(\text{OH})_6(\text{H}_2\text{O})_{12}][\text{V}_{10}\text{O}_{28}] \cdot 8\text{H}_2\text{O}$, is a new mineral (IMA2020-090) occurring in low-temperature, post-mining, secondary mineral assemblages at the Burro mine, Slick Rock district, San Miguel County, Colorado, U.S.A. Crystals of protocaseyite are saffron-yellow, thick blades, with pale orange-yellow streak, vitreous luster, brittle tenacity, curved fracture, two very good cleavages, a Mohs hardness of 2, and a density of 2.45(2) g/cm³. The optical properties of protocaseyite could be only partly determined: biaxial with $\alpha = 1.755(5)$, $\beta < 1.80$, $\gamma > 1.80$ (white light); pleochroic with X and Y yellow, Z orange ($X \approx Y < Z$). Electron-probe microanalysis and crystal-structure solution and refinement provided the empirical formula $[(\text{Al}_{3.89}\text{Mg}_{0.11}\text{Ca}_{0.02})_{\Sigma 4.02}(\text{OH})_6(\text{H}_2\text{O})_{12}][\text{H}_{0.06}\text{V}_{10}\text{O}_{28}] \cdot 8\text{H}_2\text{O}$. Protocaseyite is triclinic, $P\bar{1}$, $a = 9.435(2)$, $b = 10.742(3)$, $c = 11.205(3)$ Å, $\alpha = 75.395(7)$, $\beta = 71.057(10)$, $\gamma = 81.286(6)^\circ$, $V = 1036.4(5)$ Å³, and $Z = 1$. The crystal structure ($R_1 = 0.026$ for 4032 $I_o > 2\sigma I$ reflections) contains both the $[\text{V}_{10}\text{O}_{28}]^{6-}$ decavanadate polyoxoanion and a novel $[\text{Al}_4(\text{OH})_6(\text{H}_2\text{O})_{12}]^{6+}$ polyoxocation.

Keywords: Protocaseyite, new mineral, polyoxometalate, crystal structure, Burro mine, San Miguel County, Colorado, U.S.A.

INTRODUCTION

Low-temperature near-surface environments, particularly those containing highly charged metal cations, have the potential to form polyoxometalate ions. In recent years, extensive work on low-temperature phases associated with surficial alteration has led to the discovery of many minerals containing large polyoxometalate ions. Deposits in the Uravan mineral belt of Colorado and Utah have been a rich source of uranium and vanadium ores for more than a century. They have also been a rich source of post-mining secondary vanadium minerals that typically form in mine tunnels. The most common of these are minerals containing the decavanadate $[\text{V}_{10}\text{O}_{28}]^{6-}$ isopolyanion or its protonated or mixed-valence variants. Sherwoodite, from the Peanut mine in Montrose County, Colorado (Thompson et al. 1958), was the first mineral confirmed to contain a heteropolyanion, the $(\text{AlV}_{14}^{4+,5+}\text{O}_{40})^{n-}$ vanadoaluminate anion (Evans and Konnert 1978), which is structurally similar to the decavanadate anion. In recent years, new minerals containing variants of the Keggin heteropolyanion (Kondinski and Parac-Vogt 2018) have also been discovered in mines in the Uravan mineral belt. These include kegginite, $\text{Pb}_3\text{Ca}_3[\text{AsV}_{12}\text{O}_{40}(\text{VO})] \cdot 20\text{H}_2\text{O}$, from the Packrat mine (Mesa County, Colorado) containing a mono-capped Keggin ϵ -isomer (Kampf et al. 2017a), and bicapite,

$\text{KNa}_2\text{Mg}_2(\text{H}_2\text{PV}_{14}^{3+}\text{O}_{42}) \cdot 25\text{H}_2\text{O}$, from the Pickett Corral mine (Montrose County, Colorado) containing a bi-capped Keggin α -isomer (Kampf et al. 2019a). The Packrat mine has also yielded several new minerals containing a novel $[\text{As}^{3+}\text{V}_{12}^{4+,5+}\text{As}_6^{5+}\text{O}_{51}]^{n-}$ heteropolyanion (Kampf et al. 2016a).

The name protocaseyite links the mineral to caseyite (Kampf et al. 2020a), which contains, as a core cation, a member of the class of aluminum clusters that have sheets of Al^{3+} linked by μ_3 -OH bridges, and they are referred to colloquially as “flatimers.” This term distinguishes the sheet clusters from the more common Keggin-based structures of aluminum polyoxocations. These flatimers have only recently been discovered in nature and, in particular, in the vanadoaluminate flatimer, ideally $[(\text{V}^{5+}\text{O}_2)\text{Al}_{10}(\text{OH})_{20}(\text{H}_2\text{O})_{18}]^{11+}$, in the structure of caseyite. The new mineral protocaseyite, described in this paper, contains the $[\text{Al}_4(\text{OH})_6(\text{H}_2\text{O})_{12}]^{6+}$ tetramer, which has no μ_3 -OH bridges. We refer to it as a “flatimer,” in any case, because it is the smallest cluster that can be made stable by coordination by hydrogen bonding to a decametallate anion. We thus speculate that the tetramer in protocaseyite is genetically related to caseyite and other polynuclear Group 13 cations that could be coordinated by the decavanadate anions.

The new mineral and name have been approved by the Commission on New Minerals, Nomenclature and Classification of the International Mineralogical Association (IMA2020-090). Three cotype specimens, all micromounts, are deposited in

* E-mail: akampf@nhm.org. Orcid 0000-0001-8084-2563

† Orcid 0000-0002-1828-7033

the collections of the Natural History Museum of Los Angeles County, Los Angeles, California, U.S.A. (catalog numbers 75191, 75192, and 75193).

OCCURRENCE

Protocaseyite was found underground at the Burro mine, Slick Rock district, San Miguel County, Colorado, U.S.A. (38.04507, -108.88972). The Burro mine is the type locality for ammonio-lasalite (Kampf et al. 2018a); ammoniomatesiusite (Kampf et al. 2019b); ammoniozippeite (Kampf et al. 2018b); burroite (Kampf et al. 2017b); caseyite (Kampf et al. 2020a); metamunirite (Evans 1991); metauroxite (Kampf et al. 2020b); okieite (Kampf et al. 2020c); and uroxite (Kampf et al. 2020b). The mine is near the southern end of the Uravan mineral belt in which uranium and vanadium minerals occur together in bedded or roll-front deposits in the sandstone of the Salt Wash member of the Jurassic Morrison Formation (Carter and Gualtieri 1965; Shawe 2011). The U and V ore mineralization formed where solutions rich in U and V encountered pockets of strongly reducing solutions that had developed around accumulations of carbonaceous plant material.

The specimens of the new mineral were collected by one of the authors (J.M.). The mineral is rare. It occurs with ammoniozippeite, gypsum, postite (Kampf et al. 2012), and another potentially new Al vanadate on montroseite- and corvusite-bearing sandstone. Protocaseyite forms by oxidation of montroseite-corvusite assemblages in a moist environment. Mining operations have exposed both unoxidized and oxidized phases. Under ambient temperatures and generally oxidizing near-surface conditions, water reacts with pyrite to form aqueous solutions of relatively low pH. The various secondary vanadate phases that form depend on ambient Eh-pH conditions and the presence of other cations (e.g., NH_4^+ , Na^+ , Ca^{2+} , Mg^{2+} , Mn^{2+} , Pb^{2+}).

PHYSICAL AND OPTICAL PROPERTIES

Crystals of protocaseyite are thick blades up to 0.2 mm in length, commonly occurring in subparallel intergrowths and divergent groups (Fig. 1). The blades are elongated on $[10\bar{1}]$ and flattened on $\{111\}$. The only crystal form that could be determined with certainty is $\{111\}$; other likely forms are $\{010\}$, $\{\bar{1}\bar{1}1\}$, $\{11\bar{1}\}$, and $\{1\bar{2}1\}$ (Fig. 2). The color of the mineral is saffron yellow, its streak is pale orange yellow, and it has vitreous luster. The mineral is non-fluorescent in long- and short-wave ultraviolet light. The crystals are brittle, with curved fracture, and have a Mohs hardness of 2 based on scratch tests. There are probably two very good cleavages, one on $\{111\}$ and one along the length of the blades and at an angle to the $\{111\}$ face (possibly on $\{010\}$). The density measured by floatation in a mixture of methylene iodide and toluene is 2.45(2) g/cm^3 . The calculated density is 2.448 g/cm^3 based on the empirical formula using the single-crystal cell parameters. At room temperature, the mineral is insoluble in H_2O but is easily soluble in dilute HCl.

The small size and intergrown nature of crystals, the relatively high indices of refraction, and the extreme dispersion complicated the determination of optical properties. Conoscopic observation was inconclusive, and numerous attempts to obtain extinction measurements failed because of the extreme dispersion. The mineral is obviously biaxial, but the sign could not be determined, and $2V$ could not be measured. The only index of



FIGURE 1. Protocaseyite crystals; field of view 0.4 mm across.

refraction that could be determined (in white light) unambiguously was $\alpha = 1.755(5)$. The highest index of refraction measured on flat-lying blades was 1.800(5), and this is clearly intermediate between β and γ ; therefore, $\beta < 1.80$ and $\gamma > 1.80$. Assuming $n_{av} = 1.78$, the Gladstone-Dale compatibility $1 - (K_p/K_c)$ is 0.011 for both the empirical and ideal formulas, in the range of superior compatibility (Mandarino 2007). The pleochroism varies from yellow to orange, with only one optical direction (presumed to be Z) appearing orange; therefore, X and Y yellow, Z orange; $X \approx Y < Z$. The optical orientation could not be determined.

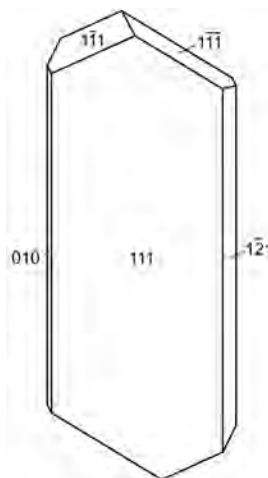


FIGURE 2. Crystal drawing of protocaseyite; clinographic projection in non-standard orientation, $[10\bar{1}]$ vertical.

TABLE 1. Chemical analytical data in wt% for protocaseyite

Constituent	Mean	Range	S.D.	Standard	Normalized
MgO	0.32	0.27–0.37	0.03	forsterite	0.28
CaO	0.09	0.07–0.10	0.01	anorthite	0.08
Al_2O_3	14.86	14.42–15.30	0.33	anorthite	12.98
V_2O_5	68.10	66.70–69.43	1.04	V_2O_5	59.51
H_2O^a					27.15
Total					100.00

^a Based upon the crystal structure with $V = 10$ and $O = 54$ apfu.

TABLE 2. Data collection and structure-refinement details for protocaseyite

Diffractometer	Bruker D8 three-circle	
X-ray radiation/source	MoK α ($\lambda = 0.71073$ Å)/rotating anode	
Temperature	293(2) K	
Structural formula	[Al ₄ (OH) ₆ (H ₂ O) ₁₂][V ₁₀ O ₂₈] \cdot 8H ₂ O	
Space group	$P\bar{1}$	
Unit-cell dimensions	$a = 9.435(2)$ Å $b = 10.742(3)$ Å $c = 11.205(3)$ Å	$\alpha = 75.395(7)^\circ$ $\beta = 71.057(10)^\circ$ $\gamma = 81.286(6)^\circ$
V	1036.4(5) Å ³	
Z	1	
Density (for above formula)	2.448 g/cm ⁻³	
Absorption coefficient	2.383 mm ⁻¹	
F(000)	760	
Crystal size	45 \times 22 \times 15 μ m	
θ range	2.81 to 27.59°	
Index ranges	-12 $\leq h \leq 12$, -13 $\leq k \leq 13$, -14 $\leq l \leq 14$	
Reflections collected/unique	30690/4786; $R_{int} = 0.0347$	
Reflections with $I > 2\sigma I$	4032	
Completeness to $\theta = 27.59^\circ$	99.9%	
Refinement method	Full-matrix least-squares on F^2	
Parameters/restraints	377/23	
GoF	1.072	
Final R indices [$I > 2\sigma I$]	$R_1 = 0.0254$, $wR_2 = 0.0689$	
R indices (all data)	$R_1 = 0.0333$, $wR_2 = 0.0716$	
Largest diff. peak/hole	+0.64/-0.33 e Å ⁻³	

Notes: $R_{int} = \sum |F_o^2 - F_c^2(\text{mean})| / \sum F_o^2$. GoF = $S = \{ \sum [w(F_o^2 - F_c^2)]^2 / (n - p) \}^{1/2}$.
 $R_1 = \sum |F_o| - |F_c| / \sum |F_o|$. $wR_2 = \{ \sum [w(F_o^2 - F_c^2)]^2 / \sum w(F_o^2) \}^{1/2}$; $w = 1 / [\sigma^2(F_o) + (aP)^2 + bP]$
 where a is 0.0297, b is 1.2951, and P is $[2F_o^2 + \text{Max}(F_o, 0)]/3$.

CHEMICAL ANALYSIS

Analyses (7 points) were done at Caltech on a JEOL 8200 electron microprobe in WDS mode. Analytical conditions were 15 kV accelerating voltage, 5 nA beam current, and 2 μ m defocused beam diameter. During vacuum deposition of the conductive carbon coat required for EPMA, protocaseyite clearly suffered loss of much of the weakly held H₂O; no further loss was detected during EPMA. The very large H₂O loss resulted in much higher concentrations of the remaining constituents than are to be expected for the fully hydrated phase; therefore, the other analyzed constituents have been normalized to provide a total of 100% when combined with the H₂O content derived from crystal-structure analysis. Analytical data are given in Table 1. The empirical formula is [(Al_{3.89}Mg_{0.11}Ca_{0.02}) Σ 4.02(OH)₆(H₂O)₁₂][H_{0.06}V₁₀O₂₈] \cdot 8H₂O based

TABLE 3. Selected bond distances (in angstroms) in protocaseyite

V1-O5	1.6764(17)	V4-O3	1.5910(18)	Al1-OH3	1.8327(18)
V1-O6	1.7048(17)	V4-O11	1.8522(17)	Al1-OH1	1.8530(18)
V1-O12	1.9194(16)	V4-O10	1.8652(17)	Al1-OH1	1.8852(18)
V1-O13	1.9337(16)	V4-O7	1.8859(17)	Al1-OH2	1.9122(18)
V1-O14	2.1049(16)	V4-O5	2.0657(17)	Al1-OW1	1.9419(19)
V1-O14	2.1300(16)	V4-O14	2.2969(16)	Al1-OW2	1.967(2)
<V1-O>	1.912	<V4-O>	1.926	<Al1-O>	1.899
V2-O1	1.6012(17)	V5-O4	1.5871(18)	Al2-OH3	1.8221(18)
V2-O7	1.8266(17)	V5-O11	1.8492(17)	Al2-OH2	1.8564(18)
V2-O8	1.8327(17)	V5-O8	1.8637(17)	Al2-OW5	1.8972(19)
V2-O12	1.9941(16)	V5-O9	1.9098(18)	Al2-OW4	1.9013(19)
V2-O13	2.0031(16)	V5-O6	2.0326(17)	Al2-OW6	1.906(2)
V2-O14	2.2424(16)	V5-O14	2.3633(16)	Al2-OW3	1.9576(19)
<V2-O>	1.917	<V5-O>	1.934	<Al2-O>	1.890
V3-O2	1.6256(18)				
V3-O9	1.7873(17)				
V3-O10	1.8305(17)				
V3-O13	1.9870(17)				
V3-O12	2.0489(16)				
V3-O14	2.2307(16)				
<V3-O>	1.918				

on 54 O apfu. The end-member formula is [Al₄(OH)₆(H₂O)₁₂][V₁₀O₂₈] \cdot 8H₂O, which requires Al₂O₃ 13.35, V₂O₅ 59.53, H₂O 27.12, total 100 wt%.

X-RAY CRYSTALLOGRAPHY AND STRUCTURE

The powder X-ray diffraction (PXRD) pattern was recorded at the Natural History Museum of Los Angeles County on a Rigaku R-Axis Rapid II microdiffractometer equipped with a curved imaging plate and monochromatized MoK α radiation. A Gandolfi-like motion on the ϕ and ω axes was used to randomize the orientation of the sample. Observed d -values and intensities were derived by profile fitting using JADE Pro software (Materials Data, Inc.). Data (in Å for MoK α) are given in Online Materials¹ Table S1.

Single-crystal X-ray studies were done at the University of Manitoba on a Bruker D8 three-circle diffractometer equipped with a rotating-anode generator (MoK α), multilayer optics, and an APEX-II detector. Structure data were collected on a crystal of protocaseyite from the holotype specimen. Satellite diffraction spots were observed, suggesting a slightly offset additional crystal domain. A second domain (37% relative volume) rotated 2.8° from the primary domain was identified using CELL_NOW (Sheldrick 2008), and the diffraction data were integrated using orientation matrices from both domains. The multi-component data were processed using TWINABS (Sheldrick 2012) such that only reflections belonging to the primary component were retained (overlapping intensity from the satellite component was subtracted). The unit-cell dimensions were obtained by least-squares refinement of 4070 reflections with $I > 10\sigma I$.

The structure was solved by direct methods using SHELXS-2013, and the structure was refined using SHELXL-2016 (Sheldrick 2015). All non-hydrogen atoms were located and refined with anisotropic-displacement parameters and full occupancies. All hydrogen-atom sites were located by difference-Fourier maps. Data collection and refinement details are given in Table 2, atom coordinates and displacement parameters in Online Materials¹ Table S2, cation-anion bond distances in Table 3, hydrogen bonds in Table 4, and a bond-valence analysis in Table 5.

DESCRIPTION AND DISCUSSION OF THE STRUCTURE

The [V₁₀O₂₈]⁶⁻ decavanadate unit

The [V₁₀O₂₈]⁶⁻ decavanadate unit is shown in ball-and-stick and polyhedral representations in Figure 3. The outer surface of the polyanion consists of 26 O atoms (O1 through O13) that are all bond-valence deficient (range = 1.62–1.90 v.u.) from the V⁵⁺ cation contributions alone (Table 5). Eight near-planar anion surfaces define the polyanion's exterior and collectively have maximal 2/m 2/m 2/m point-group symmetry. Four large anion surfaces, each containing nine anions in a hexagonal pattern, form one prism; another prism consists of four smaller triangular-shaped faces, each containing six anions (Fig. 3b). For protocaseyite, the point group symmetry of the decavanadate polyanion is $\bar{1}$, and symmetry equivalent anion faces occur in pairs on opposite sides of the polyanion (the two symmetrically distinct larger anion faces have their anions labeled in Fig. 3b).

TABLE 4. Proposed hydrogen-bonding for protocaseyite

O _b	H	O _A	O _b -O _A (Å)	H...O _A (Å)	O _b -H-O _A (°)	H-O _b -H (°)
OH1	H1	O13	2.823(2)	1.850(6)	172(4)	
OH2	H2	O9	2.904(2)	1.932(6)	172(4)	
OH3	H3	O1	2.815(2)	2.02(3)	136(3)	
		O1	2.768(2)	2.06(3)	128(3)	
OW1	H4	O8	2.668(2)	1.689(4)	176(4)	
	H5	O6	2.724(2)	1.758(9)	168(4)	110(3)
OW2	H6	O2	2.865(3)	1.906(11)	165(4)	
	H7	OW8	2.736(3)	1.831(19)	152(4)	106(3)
OW3	H8	OW8	2.764(3)	1.823(14)	160(3)	
	H9	O7	2.617(2)	1.661(11)	164(4)	113(3)
OW4	H10	O2	2.790(3)	1.833(11)	164(4)	
	H11	OW10	2.624(3)	1.647(5)	174(4)	102(3)
OW5	H12	O11	2.709(2)	1.729(3)	178(4)	
	H13	OW9	2.644(3)	1.680(10)	167(4)	106(3)
OW6	H14	O12	2.683(2)	1.711(7)	170(4)	
	H15	OW7	2.735(3)	1.823(18)	153(4)	108(3)
OW7	H16	O10	2.752(3)	1.802(16)	162(5)	
	H17	O9	3.254(3)	2.47(4)	136(4)	104(4)
		O10	2.935(3)	2.20(4)	131(4)	
		O11	3.224(3)	2.35(3)	148(4)	
OW8	H18	OW9	2.804(3)	1.88(2)	156(5)	
	H19	O5	3.089(3)	2.18(2)	154(4)	107(4)
OW9	H20	OW7	2.705(3)	1.742(13)	167(5)	
	H21	O2	3.320(3)	2.50(3)	141(4)	111(4)
OW10	H22	O8	3.377(3)	2.49(3)	150(4)	
	H22	O11	3.150(3)	2.33(3)	141(4)	
	H23	OW3	3.015(3)	2.049(11)	168(5)	121(4)

The [Al₄(OH)₆(H₂O)₁₂]⁶⁺ flatimer

The [Al₄(OH)₆(H₂O)₁₂]⁶⁺ moiety, which we refer to as a “flatimer,” is an aluminum polyoxocation consisting of a single layer of edge-sharing octahedra. It is shown in plan view and also rotated 90° about its long axis in Figures 4a and 4b. A “flatimer” is a small, approximately two-dimensional aluminum polyoxocation, and the term distinguishes such arrangements

from higher-symmetry Keggin-like ions like the more familiar [AlO₄Al₁₂(OH)₂₄(H₂O)₁₂]⁷⁺ ion. All anions (O sites) are either OH groups (shared along Al-Al edges) or H₂O groups, and the Al-flatimer in protocaseyite can be described as a corrugated unit of octahedra with flat top and bottom, and fully decorated by H atoms. To better highlight the anion configuration of this unit, only anions are drawn and connected (in plan view) in Figure 4c. Like the [V₁₀O₂₈] decavanadate unit, the Al-flatimer also has $\bar{1}$ symmetry with the center of symmetry located at its core. The Al-flatimer has two symmetrically distinct planar surfaces of anions with O_{donor}-H bonds projecting from both surfaces at high angles. The first is the top (or bottom) surface of the flatimer containing six anions bonded to the six H atoms (H1, H2, H3, H5, H6, H9), and the second is located on the side of the flatimer and contains five anions in a ring, with four of the five anions having H atoms (H3, H4, H10, H14) with their O_{donor}-H bonds at a high angle to the anion surface (Fig. 4c). The hexagonal pattern of the six H atoms on the top surface is a match for six anions on one of the large flat anion surfaces (centered by O13) of the decavanadate, and the resulting hydrogen-bond arrangement is shown in Figures 5a and 5b. The rhombic pattern of H atoms on the side of the Al-flatimer is also a match to the anion configuration on the other large flat anion surface (centered by O12) of the decavanadate, and the resulting hydrogen-bond arrangement is shown in Figures 5a and 5c.

Linkage of the decavanadate unit and the Al-flatimer

The protocaseyite structure is a layered hydrated salt. The structure consists of alternating [V₁₀O₂₈]⁶⁻ decavanadate poly-anions and [Al₄(OH)₆(H₂O)₁₂]⁶⁺ flatimers packed in a rhombic pattern, with larger-area anion surfaces perpendicular to the plane of the pattern (Fig. 6). The decavanadate and Al-flatimer

TABLE 5. Bond-valence analysis for protocaseyite

	V1	V2	V3	V4	V5	Al1	Al2	Hydrogen bonds		Σ
								donated	accepted	
O1		1.73						0.10, 0.10	1.93	
O2			1.62					0.15, 0.20, 0.10	2.07	
O3				1.77					1.77	
O4					1.79				1.79	
O5	1.41			0.49				0.10	2.00	
O6	1.30				0.54			0.20	2.04	
O7		0.94		0.80				0.25	1.99	
O8		0.92			0.85			0.20, 0.05	2.02	
O9			1.04		0.75			0.15, 0.03	1.97	
O10			0.93	0.85				0.20, 0.03	2.01	
O11				0.88	0.88			0.20, 0.03, 0.05	2.04	
O12	0.73	0.60	0.51					0.20	2.04	
O13	0.70	0.58	0.61					0.15	2.04	
O14	0.44, 0.41	0.30	0.31	0.26	0.22				1.94	
OH1						0.57, 0.53		0.85	1.95	
OH2						0.49	0.57	0.85	1.91	
OH3						0.60	0.62	0.80	2.02	
OW1						0.45		0.80, 0.80	2.05	
OW2						0.43		0.85, 0.80	2.08	
OW3							0.44	0.80, 0.75	2.09	
OW4							0.50	0.80, 0.75	2.05	
OW5							0.51	0.80, 0.75	2.06	
OW6							0.50	0.80, 0.80	2.10	
OW7								0.80, 0.91	2.11	
OW8								0.80, 0.90	2.10	
OW9								0.80, 0.90	2.15	
OW10								0.90, 0.90	2.05	
Σ	4.99	5.07	5.02	5.05	5.03	3.07	3.14			

Notes: Bond-valence parameters for V⁵⁺-O are from Brown and Altermatt (1985) and those for Al-O are from Gagné and Hawthorne (2015). Hydrogen-bond contributions estimated from O_b...O_A distances using Brown and Altermatt (1985).

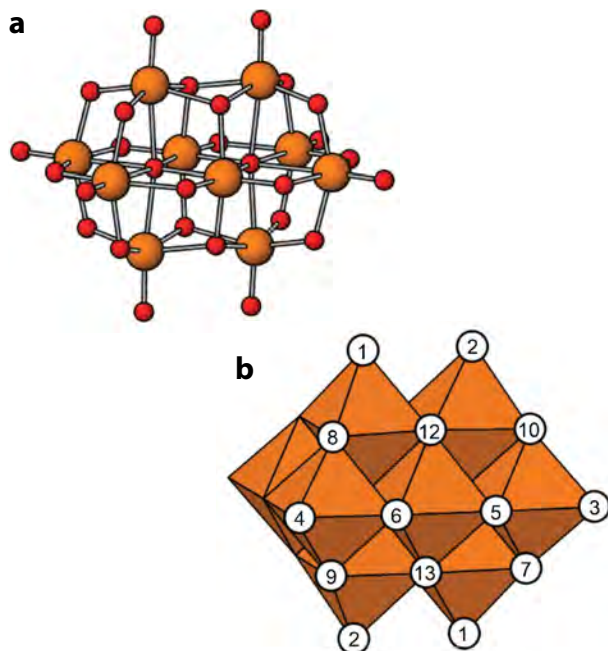


FIGURE 3. The $[V_{10}O_{28}]^{6-}$ decavanadate poly-anion represented as: (a) ball and stick, and (b) polyhedral representations. Orange circles = V atoms; red circles = O atoms; white circles = surface anions of the two largest non-symmetrically related anion faces of the poly-anion.

units link via strong hydrogen-bonding: the anion surfaces of the decavanadate, centered on the O13 anion, accept strong hydrogen-bonds along $[111]$ from the upper and lower protonated surfaces of the Al-flatimer (Fig. 6); the other two surfaces of each decavanadate-anion, centered on the O12 anion, hydrogen-bond to the protonated side of the Al-flatimer along $\bar{1}\bar{1}1$ (Fig. 6). The layer in Figure 6 links to the layers adjacent along $[111]$ via hydrogen-bonding from interstitial (H_2O) groups (Fig. 7) that link the small decavanadate surfaces (the two sloping triangular anion faces in Fig. 3b) with the ends of the Al-flatimers. Thus each $[V_{10}O_{28}]^{6-}$ decavanadate unit is surrounded by six $[Al_4(OH)_6(H_2O)_{12}]^{6+}$ flatimers, and each $[Al_4(OH)_6(H_2O)_{12}]^{6+}$ flatimer is surrounded by six $[V_{10}O_{28}]^{6-}$ decavanadate units.

Protocaseyite has a well-ordered atomic arrangement that was refined from sharp high-quality X-ray diffraction data. This is a first for a naturally occurring solid containing an extended Al-flatimer. Caseyite was the first mineral found to contain an extended Al-flatimer; however, caseyite is plagued by structural disorder that is accompanied by extensive chemical variability among its interstitial constituents (Kampf et al. 2020a). As Al-flatimers have been postulated to be important building blocks for the formation of many minerals and to occur extensively in the natural environment, the recent discovery of protocaseyite and caseyite offer important insight toward the occurrence of natural Al-flatimers in minerals. Two questions arise:

(1) Why do Al-flatimers combine with the decavanadate poly-anion in minerals?

(2) Why does protocaseyite occur as extraordinarily well-ordered crystals, whereas compounds bearing tridecamer-like Al-flatimers tend to form poor crystals if they are crystalline at all?

The following observations on the structure of protocaseyite may help to address these questions:

(1) The $[V_{10}O_{28}]^{6-}$ decavanadate poly-anion has a surface of bond-valence-deficient anions that are ideal hydrogen-bond acceptors. The entire surface of an Al-flatimer is decorated by H-atoms (either as OH groups along shared Al-Al edges or as H_2O groups). The O_{donor} anions all receive incident bond-valence from the constituent Al^{3+} ions in excess of that required to accord with the valence-sum rule assuming an $O_{donor}-H$ of 1 v.u., and hence the constituent H-atoms will form hydrogen-bonds with adjacent potential $O_{acceptor}$ anions.

(2) The decavanadate poly-anion and Al-flatimers have matching flat anion surfaces with stereochemistries suitable for the formation of linking hydrogen-bonds.

(3) If the decavanadate poly-anion(s) and Al-flatimers are stable and coexist in solution, the properties described in 1 and 2 suggest that they may crystallize by condensation involving the formation of linking hydrogen-bonds if the specific Al-flatimer provides a stereochemical match for the decavanadate poly-anion. The well-ordered protocaseyite structure, with a simple 1:1 stoichiometry of poly-anion and polycation constituents and minimal additional interstitial constituents, may represent one of the simplest and most compact decavanadate-Al-flatimer combinations to occur in crystalline form.

DECAPANADATE BOND-VALENCE ANOMALY

Reliable well-defined H positions were recovered for the (OH) and (H_2O) groups in protocaseyite from the difference-Fourier map, and the refined positions conform to well-ordered H sites exhibiting usual hydrogen-bond geometries (Table 4). The proposed bond-valence distribution among O_{donor} and $O_{acceptor}$ anions from these H positions yields bond-valence sums from 1.91 to 2.15 v.u. for 25 of the 27 anions, values that accord well with the valence-sum rule (Brown 2016), and noticeably low-bond-valence sums of 1.77 and 1.79 v.u. for the O3 and O4 anions, respectively (Table 5). These O3 and O4 anions are [1]-coordinated decavanadate surface anions that form strong vanadyl bonds and do not accept any additional bonds from interstitial constituents. Are these low-bond valences significant? How do these V4-O3 and V5-O4 vanadyl bond lengths compare to other vanadyl bonds in similar decavanadate mineral structures? Are there other decavanadate mineral structures possessing similar “naked” decavanadate surface anions that do not form any additional bonds to neighboring interstitial constituents? In recent years, the number of decavanadate mineral structures has steadily increased, and 11 of these structures (including protocaseyite) were compared to address the above questions in relation to the apparent bond-valence anomaly in protocaseyite. The selection criteria focused on well-refined structures (R values < 4%) containing precise atomic positions for all atoms (i.e., well-ordered with all H positions reliably located). Cooper et al. (2019) previously noted that highly accurate bond valences can be obtained from reliable $V^{5+}-O$ bond lengths using the bond-valence equation of Brown and Altermatt (1985). For the 11 decavanadates compared here, the calculated bond-valence sums for all V sites ranges from 4.94–5.14 v.u. and are close to the postulated V^{5+} charge. We can infer that the complementary bond valences at the coordinating O sites are

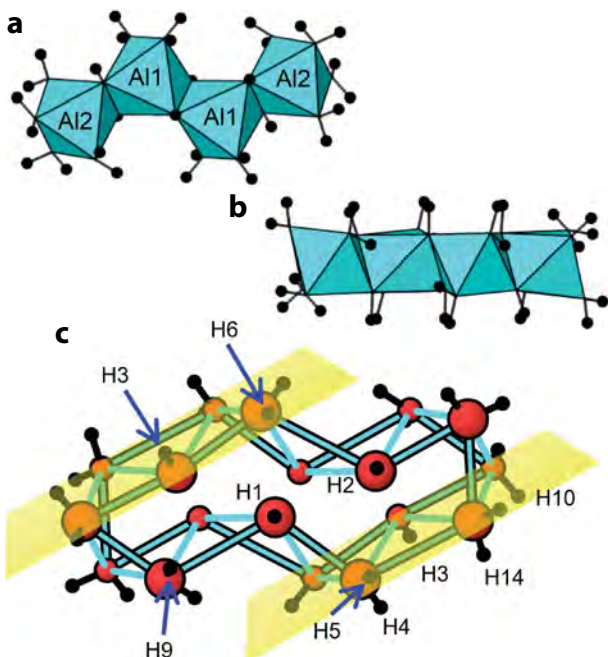


FIGURE 4. The $[\text{Al}_4(\text{OH})_6(\text{H}_2\text{O})_{12}]^{6+}$ flatimer: (a) plan view, (b) rotated 90° , (c) plan view containing only anions (larger red circles = top surface anions; smaller red circles = lower surface anions, black circles = H atoms), transparent yellow planes: highlight surface anions belonging to second largest anion surface; blue lines with black rims connect upper/lower surface anions, blue lines: connect lower to upper anions.

accurate as well, and the bond-valence sums of 1.77 and 1.79 v.u. for the O3 and O4 anions from the V^{5+} contribution alone in protocaseyite are a major departure from the valence-sum rule. Within a given $[\text{V}_{10}\text{O}_{28}]^{6-}$ polyanion, there are eight surface anions that each receive a single vanadyl bond (Fig. 8), and for the 11 structures investigated, there are 88 individual vanadyl bonds displayed on a bar graph in Figure 9. The maximum in the distribution occurs in the range $\sim 1.60\text{--}1.61$ Å, and the V4-O3 and V5-O4 distances of 1.5910 and 1.5871 Å in protocaseyite are distinctly short, in accord with the lack of interstitial bonds to these anions. A typical vanadyl bond of 1.606 Å would result in a bond-valence deficiency of ~ 0.3 v.u., whereas the shorter V4-O3 and V5-O4 distances in protocaseyite help alleviate the deficiency somewhat (i.e., reduce it to ~ 0.2 v.u.). The shortest $^{16}\text{V}^{5+}$ -O bond observed in inorganic crystals is 1.554 Å (Gagné and Hawthorne 2020), indicating that the values of ~ 1.59 Å in protocaseyite may represent a near limit of bond-length distortion for the V^{5+} polyhedra involved, where any further shortening of the vanadyl bond becomes disruptive to overall bonding within the polyanion. The eight vanadyl O atoms on a given decavanadate polyanion are the most bond-valence deficient surface anions (typically ~ 0.3 v.u. deficiency), and they are also the furthest away from the central core of the polyanion. As a result, they are ideally placed to accept additional bonds from interstitial constituents. The fact that four of these eight vanadyl O atoms on the surface of the protocaseyite decavanadate polyanion do not receive any additional bonding from interstitial constituents is quite remarkable. Of all eleven structures investigated, only

one other structure, namely postite (Kampf et al. 2012), contains a similar [1]-coordinated vanadyl oxygen; postite is also the only other decavanadate that also contains an interstitial flatimer, the $[\text{Al}_2(\text{OH})_2(\text{H}_2\text{O})_8]^{4+}$ polycation. The [1]-coordinated vanadyl oxygen in postite is at the O11 site, and the V5-O11 distance of 1.599 Å is a relatively short vanadyl distance. The [1]-coordinated vanadyl O atoms in both protocaseyite and postite are similarly situated on the equatorial girdle of the polyanion (Fig. 8). Both protocaseyite and postite have short distances between the flat anion surfaces of decavanadate polyanions and flat aluminate-hydrate polycations, which are bridged by H bonds. In turn, this may lead to relatively inaccessible dead zones near the fringes of these zones of H bonds, where the ability of other interstitial components to bond to some decavanadate surface anions (i.e., outermost vanadyl O atoms) is sterically inhibited. More equant interstitial constituents [e.g., $\text{Na}(\text{H}_2\text{O})_6$ clusters or small (H_2O) groups] are more suited to provide a complete distribution of weak bonding to all decavanadate surface anions without major steric interference. Although only a few structures with well-behaved decavanadate-flatimer units are known, the interaction of these two types of unit apparently leads to under-

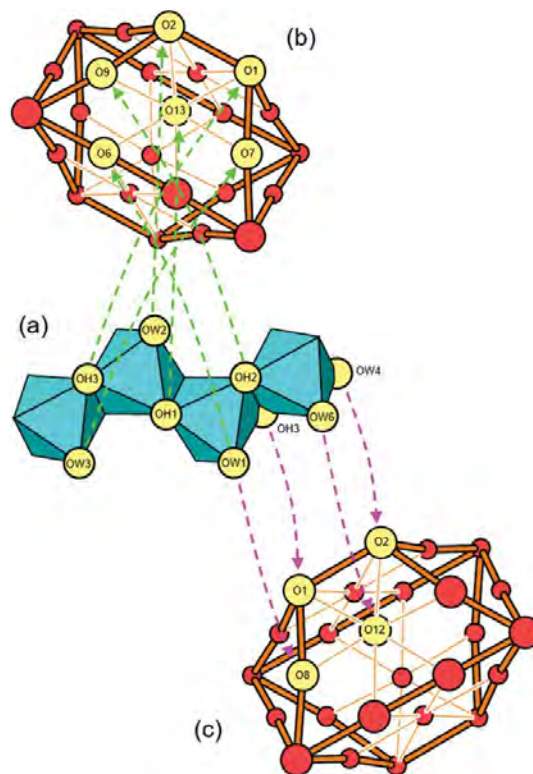


FIGURE 5. Hydrogen bonding between: (a) upper surface OD anions of the $[\text{Al}_4(\text{OH})_6(\text{H}_2\text{O})_{12}]^{6+}$ flatimer, and (b) OA anions of the O13-centered face; and between side OD anions of the $[\text{Al}_4(\text{OH})_6(\text{H}_2\text{O})_{12}]^{6+}$ flatimer to (c) OA anions of the O12-centered face of the $[\text{V}_{10}\text{O}_{28}]^{6-}$ decavanadate polyanion. Decavanadate polyanions represented by surface anions only (yellow and red circles), with large circles as upper surface anions, polyanion surface junctures marked with orange lines containing black rims; pale yellow shaded circles = OD and OA anions involved in hydrogen bond coupling (green, pink dashed lines).

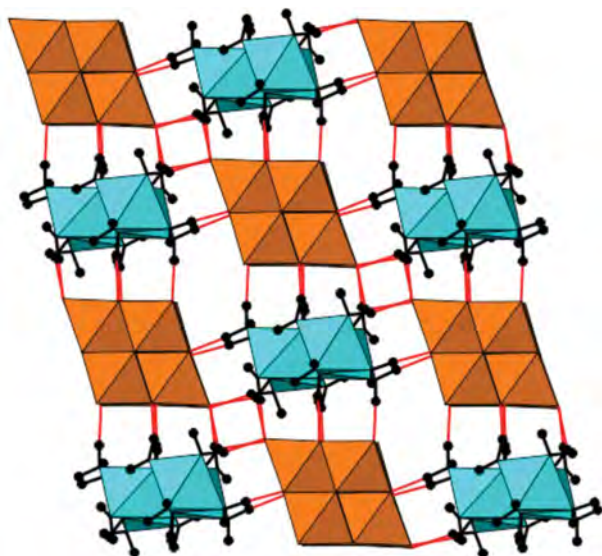


FIGURE 6. The $[V_{10}O_{28}]^{6-} - [Al_4(OH)_6(H_2O)_{12}]^{6+}$ layer in protocaseyite projected down $[1\bar{2}1]$. Hydrogen bonds are shown as red lines. The view is approximately parallel to the plane of the layer. Interstitial H_2O groups are not shown.

saturated surface anions on the decavanadate polyanion. With a much larger $[V^{5+}O_2Al_{10}(OH)_{20}(H_2O)_{18}]^{11+}$ flatimer, caseyite invokes a novel mechanism by which it alters the bonding landscape at the periphery of the flatimer and may help to prevent a local dead zone from occurring via inversion of the steric argument: adding a $V^{5+}O_2(OH)_4$ octahedron with two outer vanadyl O atoms onto the margin of the flatimer removes any sterically interfering H atoms projecting outward from an H_2O group and

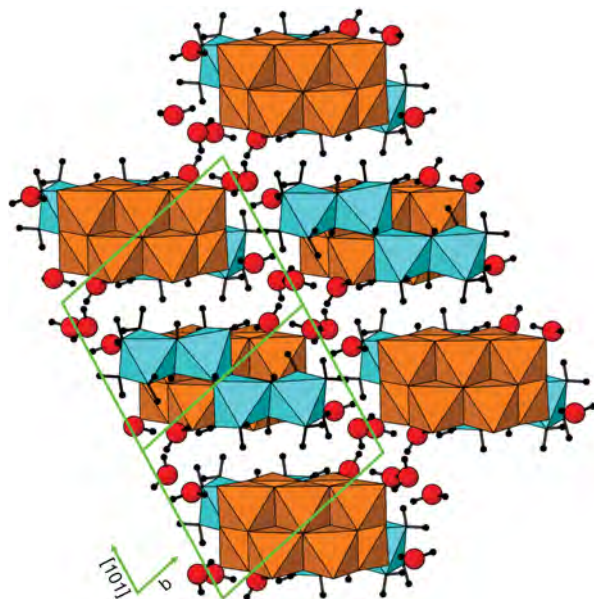


FIGURE 7. The structure of protocaseyite projected down $[10\bar{1}]$. The O atoms of the interstitial (H_2O) groups are shown as red circles. The outline of the unit cell is shown in green.

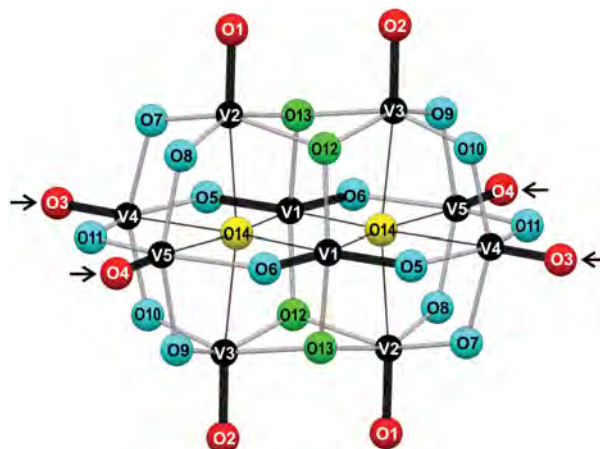


FIGURE 8. The $[V_{10}O_{28}]^{6-}$ decavanadate polyanion in protocaseyite with the “naked” O3 and O4 atoms indicated with arrows. Note that the “naked” O11 atom in postite in is the same position as the O4 atom in protocaseyite. V atoms = black circles; [1]-coordinated O atoms = red circles; [2]-coordinated O atoms = blue circles; [3]-coordinated O atoms = green circles; [6]-coordinated O atoms = yellow circles; V-O_{vanadyl} bonds = thick black line; V-O_{trans} bonds = thin black line; V-O_{equatorial} bonds = gray shaded line.

allowing other interstitial constituents to bond to under-bonded anions (Kampf et al. 2020a).

IMPLICATIONS

Aluminum is the third most abundant element (after oxygen and silicon) in the Earth’s crust. Although clay minerals generally maintain low-Al concentrations in surface waters, the solubilities can become high in acidic solutions, such as those found near exposed ore deposits. Generally, millimolar concentrations of total dissolved aluminum are required for formation of multimeric ions like the $[AlO_4Al_{12}(OH)_{24}(H_2O)_{12}]^{7+}$, and these may actually

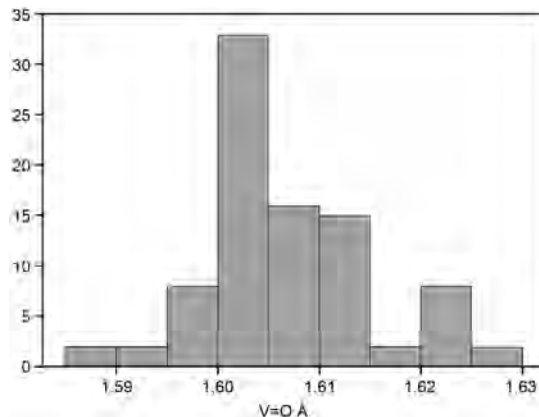


FIGURE 9. The 88 vanadyl bonds for the [1]-coordinated O atoms of 11 decavanadate mineral structures: ammoniolasaltite (Kampf et al. 2018a), huemulite (Colombo et al. 2011), hummerite (Hughes et al. 2002), kokinosite (Kampf et al. 2014), lasaltite (Hughes et al. 2008), magnesiofascioite (Kampf and Steele 2008), okieite (Kampf et al. 2020c), pascoite (Hughes et al. 2005), postite (Kampf et al. 2012), protocaseyite (this study), and wernerbaurite (Kampf et al. 2016b).

be metastable relative to monomer ions and solids.

It is difficult to prove unequivocally that an oxide ion cluster found in a mineral previously existed separately as an ion in the precipitating solution. Such proof generally requires isotope-tracing experiments or dynamic spectroscopy. Clusters in a mineral could polymerize at the interface during mineral growth and have no existence separately in solution. At the opposite extreme, isotope-tracing experiments have shown that large cluster ions of inert metals, like Group V and VI polyoxometalates, clearly form minerals when rates of ligand exchange are much slower than rates of mineral growth (see Spiccia and Casey 2007). Even aquated monomer ions form solids as intact solvated ions when the rates of ligand exchange are much slower than the rates of mineral growth. Such would be found, for example, for $[\text{Rh}(\text{H}_2\text{O})_6]^{3+}$ ions where Rh-bonded waters of hydration have an average lifetime of two years in the inner-coordination sphere of the metal (Richens 1997). The metal-hydroxide solid $\text{Rh}(\text{H}_2\text{O})_3(\text{OH})_3$ forms instantaneously when the ion is thrice deprotonated, but the inner-sphere waters never move out of their positions bonded to the Rh^{3+} (see Spiccia and Marty 1986; Crimp and Spiccia 1995; Spiccia 2004).

However, proving this point is particularly difficult for metal cations like Al^{3+} , where the rates of ligand exchange are on the same time scale as, or faster than, rates of mineral growth. Rates of ligand substitution at Al^{3+} centers are seconds to microseconds and are particularly fast if the metal is partly hydrolyzed (Casey 2006). Thus, it is completely possible that the flatimers polymerized at the growing mineral interface and have no separate lifetime as ions in solution. Aluminum nanoclusters are rarely found as isolated entities in minerals. A noteworthy counterexample is the $\alpha\text{-Al}_{13}$ Keggin cluster that forms part of the framework structure of zunyite (Louisnathan and Gibbs 1972; Baur and Ohta 1982).

The core cation in caseyite has a tridecamer structure that is well known from synthesis (Wang et al. 2011; Gatlin et al. 2008) and is referred to as a “flatimer” to distinguish it from Keggin structures. The novel $[\text{Al}_4(\text{OH})_6(\text{H}_2\text{O})_{12}]^{16-}$ flatimer in protocaseyite is the smallest possible Al-flatimer that can assemble with $[\text{V}_{10}\text{O}_{28}]^{16-}$ polyanions in a 1:1 stoichiometry. If a smaller Al-flatimer were present (e.g., $[\text{Al}_3(\text{OH})_4(\text{H}_2\text{O})_{10}]^{5-}$), then a 1:1 Al-flatimer-to-decavanadate stoichiometry could assemble only with an additional charged (i.e., 1+) interstitial constituent present. In this sense, the “proto” designator distinguishes protocaseyite as the simple proto-type structure from which all other Al-flatimer-decavanadate structures are hierarchical derivatives. Larger Al-flatimers are expected to be identified in future studies, probably along with greater variability in additional charged interstitial constituents and possible replacement of some Al^{3+} with other highly charged cations, e.g., V^{5+} as in caseyite.

There have been many synthesis studies of polyoxometalate anions and, more rarely, polyoxometalate cations, in recent years, largely because of their potential technological uses. The occurrence of both polyoxometalate anions and polyoxometalate cations in the same crystal structure (e.g., protocaseyite, caseyite) suggests that co-crystallization of these units could provide a strategy for crystallization of synthetic phases containing species that are in aqueous solution but not readily incorporated into crystalline hydroxy-hydrated aluminates.

ACKNOWLEDGMENTS AND FUNDING

Two anonymous reviewers are thanked for constructive comments, which improved the manuscript. This study was funded, in part, by the John Jago Trelawney Endowment to the Mineral Sciences Department of the Natural History Museum of Los Angeles County.

REFERENCES CITED

- Baur, W.H., and Ohta, T. (1982) The Si_5O_{16} pentamer in zunyite refined and empirical relations for individual silicon–oxygen bonds. *Acta Crystallographica*, B38, 390–401.
- Brown, I.D. (2016) *The Chemical Bond in Inorganic Chemistry. The Bond Valence Model*, 2nd ed. Oxford University Press.
- Brown, I.D., and Altermatt, D. (1985) Bond-valence parameters from a systematic analysis of the inorganic crystal structure database. *Acta Crystallographica*, B41, 244–247.
- Carter, W.D., and Gualtieri, J.L. (1965) Geology and uranium–vanadium deposits of the La Sal quadrangle, San Juan County, Utah, and Montrose County, Colorado. United States Geological Survey Professional Paper, 508.
- Casey, W.H. (2006) Large aqueous aluminum-hydroxide molecules. *Chemical Reviews*, 106, 1–16.
- Colombo, F., Baggio, R., and Kampf, A.R. (2011) The crystal structure of the elusive huemulite. *Canadian Mineralogist*, 49, 849–864.
- Cooper, M.A., Hawthorne, F.C., Kampf, A.R., and Hughes, J.M. (2019) Determination of $\text{V}^{4+}:\text{V}^{5+}$ ratios in the $[\text{V}_{10}\text{O}_{28}]^{16-}$ decavanadate polyanion. *Canadian Mineralogist*, 57, 235–244.
- Crimp, S.J., and Spiccia, L. (1995) Characterization of three active rhodium(III) hydroxides. *Australian Journal of Chemistry*, 48, 557–566.
- Evans, H.T. Jr. (1991) Metamunirite, a new anhydrous sodium metavanadate from San Miguel County, Colorado. *Mineralogical Magazine*, 55, 509–513.
- Evans, H.T. Jr., and Konner, J.A. (1978) The crystal chemistry of sherwoodite, a calcium 14-vanadoaluminate heteropoly complex. *American Mineralogist*, 63, 863–868.
- Gagné, O.C., and Hawthorne, F.C. (2015) Comprehensive derivation of bond-valence parameters for ion pairs involving oxygen. *Acta Crystallographica*, B71, 562–578.
- Gagné, O.C., and Hawthorne, F.C. (2020) Bond-length distributions for ions bonded to oxygen: Results for the transition metals and quantification of the factors underlying bond-length variation in inorganic solids. *IUCr*, 7, 581–629.
- Gatlin, J.T., Mensinger, Z.L., Zakharov, L.N., MacInnes, D., and Johnson, D.W. (2008) Facile synthesis of the tridecameric Al_{13} nanocluster $\text{Al}_{13}(\mu_3\text{-OH})_6(\mu\text{-OH})_{18}(\text{H}_2\text{O})_{24}(\text{NO}_3)_{15}$. *Inorganic Chemistry*, 47, 1267–1269.
- Hughes, J.M., Schindler, M., Rakovan, J., and Cureton, F.E. (2002) The crystal structure of hummerite, $\text{KMg}(\text{V}_5\text{O}_{14})\cdot 8\text{H}_2\text{O}$: bonding between the $[\text{V}_{10}\text{O}_{28}]^{16-}$ structural unit and the $\{\text{K}_2\text{Mg}_2(\text{H}_2\text{O})_{16}\}^{6+}$ interstitial complex. *Canadian Mineralogist*, 40, 1429–1435.
- Hughes, J.M., Schindler, M., and Francis, C.A. (2005) The $C2/m$ disordered structure of pascoite, $\text{Ca}_3(\text{V}_{10}\text{O}_{28})\cdot 17\text{H}_2\text{O}$. *Canadian Mineralogist*, 43, 1379–1386.
- Hughes, J.M., Wise, W.S., Gunter, M.E., Morton, J.P., and Rakovan, J. (2008) Lasalite, $\text{Na}_2\text{Mg}_2[\text{V}_{10}\text{O}_{28}]\cdot 20\text{H}_2\text{O}$, a new decavanadate mineral species from the Vanadium Queen Mine, La Sal District, Utah: Description, atomic arrangement, and relationship to the pascoite group of minerals. *Canadian Mineralogist*, 46, 1365–1372.
- Kampf, A.R., and Steele, I.M. (2008) Magnesio-pascoite, a new member of the pascoite group: Description and crystal structure. *Canadian Mineralogist*, 46, 679–686.
- Kampf, A.R., Hughes, J.M., Marty, J., and Nash, B. (2012) Postite, $\text{Mg}(\text{H}_2\text{O})_6\text{Al}_2(\text{OH})_2(\text{H}_2\text{O})_8(\text{V}_{10}\text{O}_{28})\cdot 13\text{H}_2\text{O}$, a new mineral species from the La Sal mining district, Utah: Crystal structure and descriptive mineralogy. *Canadian Mineralogist*, 50, 45–53.
- Kampf, A.R., Hughes, J.M., Nash, B.P., and Marty, J. (2014) Kokinosite, $\text{Na}_2\text{Ca}_2(\text{V}_{10}\text{O}_{28})\cdot 24\text{H}_2\text{O}$, a new decavanadate mineral species from the St. Jude mine, Colorado: crystal structure and descriptive mineralogy. *Canadian Mineralogist*, 52, 15–25.
- (2016a) Vanarsite, packratite, morrisonite, and gatewayite: four new minerals containing the $[\text{As}^{3+}\text{V}_2^{4+5+}\text{As}_5^6\text{O}_{31}]$ heteropolyanion, a novel polyoxometalate cluster. *Canadian Mineralogist*, 54, 145–162.
- Kampf, A.R., Hughes, J.M., Nash, B.P., Marty, J., Cooper, M.A., Hawthorne, F.C., Karpenko, V.Y., Pautov, L.A., and Agakhanov, A.A. (2016b) Revision of the formulas of wernerbaurite and schindlerite: Ammonium- rather than hydronium-bearing decavanadate minerals. *Canadian Mineralogist*, 54, 555–558.
- Kampf, A.R., Hughes, J.M., Nash, B.P., and Marty, J. (2017a) Kegginitite, $\text{Pb}_2\text{Ca}_3[\text{AsV}_{12}\text{O}_{40}(\text{VO})]\cdot 20\text{H}_2\text{O}$, a new mineral with an ϵ -isomer of the Keggin anion. *American Mineralogist*, 102, 461–465.
- Kampf, A.R., Nash, B.P., Marty, J., and Hughes, J.M. (2017b) Burroite, $\text{Ca}_2(\text{NH}_4)_2(\text{V}_{10}\text{O}_{28})\cdot 15\text{H}_2\text{O}$, a new decavanadate mineral from the Burro mine, San Miguel County, Colorado. *Canadian Mineralogist*, 55, 473–481.
- Kampf, A.R., Nash, B.P., Adams, P.M., Marty, J., and Hughes, J.M. (2018a) Ammoniolasalite, $(\text{NH}_4)_2\text{Mg}_2(\text{H}_2\text{O})_{20}[\text{V}_{10}\text{O}_{28}]$, a new decavanadate species

- from the Burro mine, Slick Rock district, Colorado. *Canadian Mineralogist*, 56, 859–869.
- Kampf, A.R., Plášil, J., Olds, T.A., Nash, B.P., and Marty, J. (2018b) Ammoniozippeite, a new uranyl sulfate from the Blue Lizard mine, San Juan County, Utah, and the Burro mine, San Miguel County, Colorado, U.S.A. *Canadian Mineralogist*, 56, 235–245.
- Kampf, A.R., Hughes, J.M., Nash, B.P., and Marty, J. (2019a) Bicapite, $\text{KNa}_2\text{Mg}_2(\text{H}_2\text{PV}_{14}\text{O}_{42})\cdot 25\text{H}_2\text{O}$, a new mineral with a bicapped Keggin anion from the Pickett Corral mine, Montrose County, Colorado, USA. *American Mineralogist*, 104, 1851–1856.
- Kampf, A.R., Plášil, J., Nash, B.P., and Marty, J. (2019b) Ammoniomathesiusite, a new uranyl sulfate-vanadate mineral from the Burro mine, San Miguel County, Colorado, U.S.A. *Mineralogical Magazine*, 83, 115–121.
- Kampf, A.R., Cooper, M.A., Hughes, J.M., Nash, B.P., Marty, J., and Hawthorne, F.C. (2020a) Caseyite a new mineral containing a variant of the flat- Al_{13} polyoxometalate cation. *American Mineralogist*, 105, 123–131.
- Kampf, A.R., Plášil, J., Nash, B.P., Némec, I., and Marty, J. (2020b) Uroxite and metauroxite, the first two uranyl-oxalate minerals. *Mineralogical Magazine*, 84, 131–141.
- Kampf, A.R., Adams, P.M., Nash, B.P., Marty, J., and Hughes, J.M. (2020c) Okieite, $\text{Mg}_3[\text{V}_{10}\text{O}_{28}]\cdot 28\text{H}_2\text{O}$, a new decavanadate mineral from the Burro mine, Slick Rock mining district, San Miguel County, Colorado, U.S.A. *Canadian Mineralogist*, 58, 125–135.
- Kondinski, A., and Parac-Vogt, T.N. (2018) Keggin Structure, Quo Vadis? *Frontiers in Chemistry*, 6, 346 Article 346.
- Louisnathan, S.J., and Gibbs, G.V. (1972) Aluminum-silicon distribution in zunyite. *American Mineralogist*, 57, 1089–1108.
- Mandarino, J.A. (2007) The Gladstone–Dale compatibility of minerals and its use in selecting mineral species for further study. *Canadian Mineralogist*, 45, 1307–1324.
- Richens, D.T. (1997) *Chemistry of Aqua Ions*. J. Wiley.
- Shawe, D.R. (2011) Uranium-vanadium deposits of the Slick Rock district, Colorado. United States Geological Survey Professional Paper, 576-F.
- Sheldrick, G.M. (2008) CELL_NOW, Version 2008/4. Georg-August-Universität Göttingen: Göttingen, Germany.
- (2012) TWINABS 2012/1. Georg-August-University Göttingen, Göttingen, Germany.
- (2015) Crystal Structure refinement with SHELX. *Acta Crystallographica*, C71, 3–8.
- Spiccia, L. (2004) Homopolynuclear and heteropolynuclear Rh(III) aqua ions—A review. *Inorganica Chimica Acta*, 357, 2799–2817.
- Spiccia, L., and Casey, W.H. (2007) Synthesis of experimental models for molecular inorganic geochemistry—A review with examples. *Geochimica et Cosmochimica Acta*, 71, 5590–5604.
- Spiccia, L., and Marty, W. (1986) The fate of active chromium hydroxide, $\text{Cr}(\text{OH})_3\cdot 3\text{H}_2\text{O}$, in aqueous suspension. Study of the chemical changes involved in its aging. *Inorganic Chemistry*, 25, 266–271.
- Wang, W., Wentz, K.M., Hayes, S.E., Johnson, D.W., and Keszler, D. (2011) Synthesis of the hydroxide cluster $[\text{Al}_{13}(\mu_3\text{-OH})_6(\mu\text{-OH})_{18}(\text{H}_2\text{O})_{24}]^{15+}$ from an aqueous solution. *Inorganic Chemistry*, 50, 4683–4685.

MANUSCRIPT RECEIVED MARCH 17, 2021

MANUSCRIPT ACCEPTED JUNE 16, 2021

MANUSCRIPT HANDLED BY G. DIEGO GATTA

Endnote:

¹Deposit item AM-22-68059, Online Materials. Deposit items are free to all readers and found on the MSA website, via the specific issue's Table of Contents (go to http://www.minsocam.org/MSA/AmMin/TOC/2022/Jun2022_data/Jun2022_data.html). The CIF has been peer reviewed by our Technical Editors.